

Article

Solid-State Self-Assembly of a Linear Hexanuclear Copper(II) Oxamate Complex with Alternating Antiferro- and Ferromagnetic Coupling

Ana Luísa A. Lage¹, Luísa A. Ribeiro¹ , Antônio C. Dorigueto², Carlos B. Pinheiro³, Wallace C. Nunes⁴, Emerson F. Pedroso⁵ and Cynthia L. M. Pereira^{1,*} 

¹ Departamento de Química, Instituto de Ciências Exatas, Universidade Federal de Minas Gerais, Av. Antônio Carlos 6627, Belo Horizonte 31270-901, MG, Brazil

² Instituto de Química, Universidade Federal de Alfenas, Alfenas 37133-840, MG, Brazil

³ Departamento de Física, Instituto de Ciências Exatas, Universidade Federal de Minas Gerais, Av. Antônio Carlos 6627, Belo Horizonte 31270-901, MG, Brazil

⁴ Instituto de Física, Universidade Federal Fluminense, Av. Gal. Milton Tavares de Souza, s/nº, Niterói 24210-346, RJ, Brazil

⁵ Centro Federal de Educação Tecnológica de Minas Gerais, Av. Amazonas 5855, Belo Horizonte 30421-169, MG, Brazil

* Correspondence: cynthialopes@ufmg.br

Abstract: In this work, we describe the synthesis, crystal structure and magnetic properties of the neutral hexacopper(II) complex of formula $\{[\text{Cu}(\text{bpc})]_2[\text{Cu}(\text{dmopba})(\text{H}_2\text{O})]\}_2 \cdot 4\text{H}_2\text{O}$ (**1**), where Hbpc = bis(2-pyridylcarbonyl)-amide and dmopba = 4,5-dimethyl-1,2-phenylenebis(oxamato). Single crystals of **1** were obtained from the stoichiometric reaction (1:2 molar ratio) of the mononuclear copper(II) complexes $(n\text{-Bu}_4\text{N})_2[\text{Cu}(\text{dmpba})]$ and $[\text{Cu}(\text{bpca})(\text{H}_2\text{O})_2]\text{NO}_3 \cdot 2\text{H}_2\text{O}$ through slow diffusion techniques in water as a solvent. The crystal structure of **1** shows that two neutral $\{[\text{Cu}(\text{bpc})]_2[\text{Cu}(\text{dmopba})(\text{H}_2\text{O})]\}$ trinuclear units are connected through double out-of-plane copper to outer carboxylate oxygen atoms resulting in a unique oxamate-bridged linear hexanuclear complex. Hydrogen bonds among adjacent entities involving the non-coordinated water molecules result in a supramolecular 3D network. Magnetic measurements on **1** show the occurrence of moderate antiferromagnetic intratrinuclear interactions between the copper(II) ions from the $[\text{Cu}(\text{bpca})]^+$ and $[\text{Cu}(\text{dmopba})(\text{H}_2\text{O})]^{2-}$ fragments across the oxamate bridge and a weak intertrinuclear ferromagnetic interaction between the copper(II) ions that occurs between the two central $[\text{Cu}(\text{bpca})]^+$ fragments mediated by the carboxylate groups from the oxamate bridge $[J = -31.96(2) \text{ cm}^{-1}$ and $J' = +1.34(2) \text{ cm}^{-1}$; $H = J (S_1 \cdot S_2 + S_2 \cdot S_3 + S_1' \cdot S_2' + S_2' \cdot S_3') + J' (S_1 \cdot S_1')]$.

Keywords: oxamate; copper(II); crystal engineering; supramolecular chemistry; magnetic properties



Citation: Lage, A.L.A.; Ribeiro, L.A.; Dorigueto, A.C.; Pinheiro, C.B.; Nunes, W.C.; Pedroso, E.F.; Pereira, C.L.M. Solid-State Self-Assembly of a Linear Hexanuclear Copper(II) Oxamate Complex with Alternating Antiferro- and Ferromagnetic Coupling. *Magnetochemistry* **2022**, *8*, 116. <https://doi.org/10.3390/magnetochemistry8100116>

Academic Editors: Kamil Gareev and Ksenia Chichay

Received: 11 September 2022

Accepted: 21 September 2022

Published: 28 September 2022

Publisher's Note: MDPI stays neutral with regard to jurisdictional claims in published maps and institutional affiliations.



Copyright: © 2022 by the authors. Licensee MDPI, Basel, Switzerland. This article is an open access article distributed under the terms and conditions of the Creative Commons Attribution (CC BY) license (<https://creativecommons.org/licenses/by/4.0/>).

1. Introduction

Today, crystal engineering and supramolecular chemistry are important areas involving the synthesis of interesting molecules with desirable properties and with the potential to develop new materials and devices for different areas, such as sensing [1] phase transitions [2], supramolecular catalysis [3], antitumor agents [4], advanced materials for energy storage [5], photochromism [6], magnetic resonance imaging (MRI) [7], and magnetic materials [8], for instance. The control of the self-assembly of neutral or charged molecules and counterions is one of the areas studied by scientists that work with the synthesis of new compounds [9]. All factors that can affect the obtention of a molecular compound should be studied and shared with other scientists envisaging not only the rationalization and reproducibility but also the development of new experimental techniques for the obtention of interesting compounds, preferentially with high purity and crystallinity. It is imperative to rationalize the factors that can govern molecular self-assembly and crystal packing,

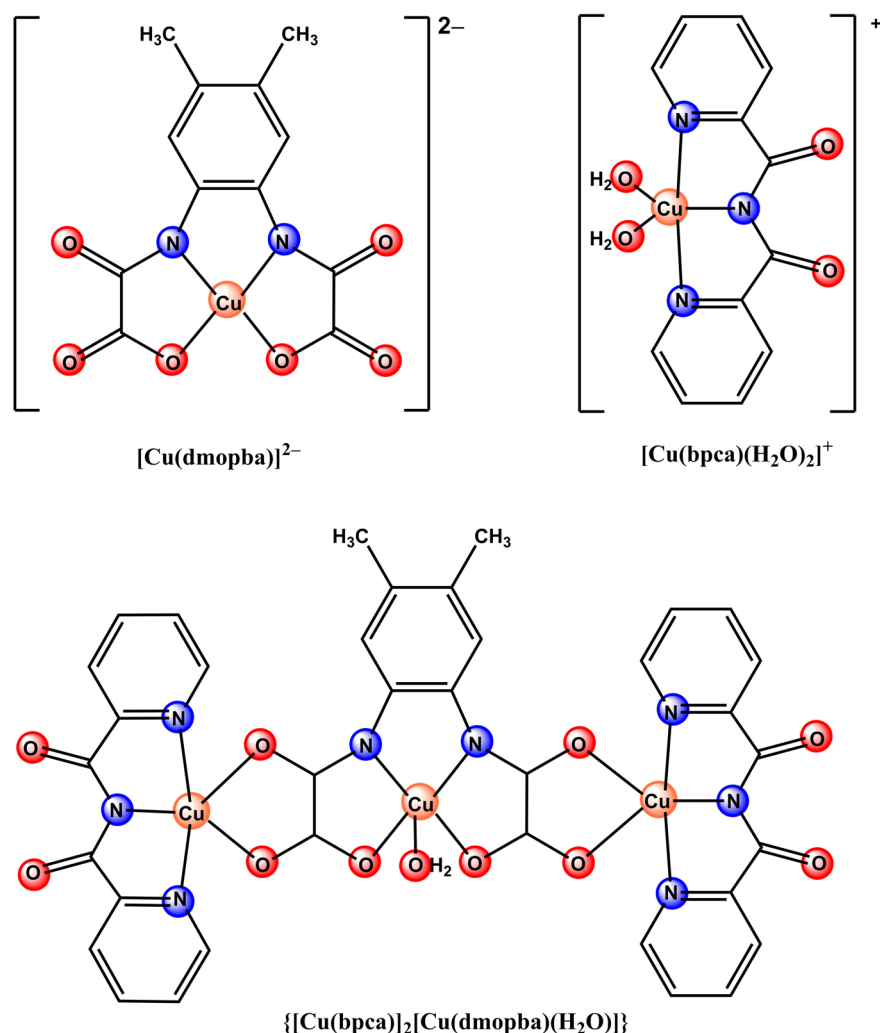
providing the literature with a variety of examples of how, e.g., temperature, stoichiometry, the kind of solvent (that favors the self-assembly process or not), pH, concentration of reactants, moisture, visible or UV light irradiation, and type of counterion play a tentative role in understanding the crystal growth mechanism [10,11].

Along this line, we have been working with molecule-based magnetic materials built with oxamate ligands [12]. The strategy consists in using a transition metal complex with a polychelating oxamate ligand as a building block toward other transition or rare earth metal ions and complexes, envisaging the obtention of the desired molecular architecture with a predictable structure and magnetic properties.

The great versatility of polychelating oxamate ligands in the coordination of transition metal ions has been described in several reports [12–14]. Due to the presence of several sites of coordination and bridging nature [14], they can be used to form discrete mono- [15,16], di- [17], and trinuclear species [18], up to deca- or dodecanuclear nanowheel systems [19,20], as well as extended chains [21], planes [22], and 3D networks [23], so-called metal–organic frameworks [12,13,24]. Supramolecular chemistry plays an important role in this synthetic strategy because it can also drive the dimensionality of the network through coordinative interactions, hydrogen bonds, the interaction between cations and anions, Van der Waals forces, and π – π stacking interactions, to cite some examples [25,26]. Additionally, depending on the nature of the metal ion, counterion, solvent, or network dimensionality, different compounds with potential use in different areas of knowledge have been described, beyond magnetic materials, such as antitumor agents [27–29], catalysts for homogeneous or heterogeneous reactions [30,31], gas adsorption [32,33], or luminescence [34,35], for instance.

Focusing on molecule-based magnetic materials made of homotrimeric copper(II) oxamate systems, there are a few examples of discrete units described in the literature [18,36–39]. These compounds were built using the self-assembly of discrete mononuclear oxamate complexes and copper(II) complexes acting as blocking ligands such as *N,N,N',N'*-tetramethylethylenediamine (tmen) [36–39], *N,N,N',N'',N'''*-pentaethyldiethylenetriamine (pet), *N,N,N',N'',N'''*-pentamethyldiethylenetriamine (pmd), bis(3-aminopropyl)amine (bapa), and 2,2':2',6''-terpyridine (terpy) [36]. The strength of magnetic coupling (J) through oxamate bridges can be modified depending on the type of blocking ligand. In the case of homotrimeric oxamate copper(II) complexes with bidentate blocking ligands, it was demonstrated that a strong antiferromagnetic coupling ($J \sim -350 \text{ cm}^{-1}$) is expected when all three copper(II) ions are square planar with an almost coplanar disposition of the metal basal planes. When the terminal copper(II) ions with a tridentate blocking ligand have a square pyramidal or a bipyramidal trigonal geometry, the antiferromagnetic coupling through the oxamate bridge reduces in intensity (J varying from -379 to -84 cm^{-1}) [36–39].

In this work, we present the synthesis, structural characterization, and magnetic properties of a novel hexacopper(II) complex of formula $\{[\text{Cu}(\text{bpca})]_2[\text{Cu}(\text{dmopba})(\text{H}_2\text{O})]\}_2 \cdot 4\text{H}_2\text{O}$ (**1**) resulting from the molecular self-assembly in the solid state of two such tricopper(II) oxamate complexes prepared from the mononuclear $[\text{Cu}(\text{dmopba})]^{2-}$ and $[\text{Cu}(\text{bpca})(\text{H}_2\text{O})_2]^+$ precursors in water (Scheme 1). To our knowledge, **1** is one of the rare examples of homometallic hexanuclear copper(II) oxamate complexes with alternating antiferro- and ferromagnetic interactions reported in the literature, the vast majority of them featuring antiferromagnetic interactions [40–42].



Scheme 1. Chemical formula of the trinuclear copper(II) oxamate basic unit $\{[\text{Cu}(\text{bpca})_2][\text{Cu}(\text{dmopba})(\text{H}_2\text{O})]\}$ resulting from the self-assembly of the $[\text{Cu}(\text{dmopba})]^{2-}$ anion and $[\text{Cu}(\text{bpca})(\text{H}_2\text{O})_2]^+$ cations in water.

2. Materials and Methods

All chemicals used in this work were purchased from the analytical grade of Sigma Aldrich, and they were used as received. The diethyl ester derivatives of the 4,5-dimethyl-1,2-phenylenebis(oxamato) ligand ($\text{Et}_2\text{H}_2\text{dmopba}$) [43,44] and $[\text{Cu}(\text{bpca})(\text{H}_2\text{O})_2]\text{NO}_3 \cdot 2\text{H}_2\text{O}$ [45] were obtained according to literature methods. Elemental analyses (C, H, N) were carried out with a Perkin-Elmer 2400 elemental analyzer. Atomic absorption spectrometry was used to determine the copper contents with a Hitachi Z-8200 Polarized Atomic Absorption Spectrophotometer. The Fourier-transformed infrared spectrum (FTIR) of **1** was recorded on a Perkin Elmer 882 spectrophotometer in the range 4000 and 400 cm^{-1} using dry KBr pellets (Figure S1, Supplementary Materials). Thermal analysis (TG and DTG curves) of **1** was carried out in alumina crucible sample holding on a Shimadzu TGA-60 using a dynamic nitrogen atmosphere (Figure S2, Supplementary Materials). The powder X-ray diffraction pattern (PXRD) of **1** was recorded at room temperature on a Rigaku/Geirgflex diffractometer. Diffraction data were collected using monochromatic Cu-K radiation in Bragg/Brentano mode (deg s^{-1}). Using the crystal data retrieved from the CIF file, a simulated PXRD pattern of **1** was generated with the Mercury[®] software (2022.1.0, Build 343014, Mercury software, Kildare, Ireland) [46] (Figure S3, Supplementary Materials).

2.1. Synthesis of $(n\text{-Bu}_4\text{N})_2[\text{Cu}(\text{dmopba})]$

This compound was synthesized similarly to what was previously described [43,44]: a 40% water solution of $n\text{-Bu}_4\text{NOH}$ (24.5 mL, 23.7 mmol) was added dropwise to a suspension containing $\text{Et}_2\text{H}_2\text{dmopba}$ (1.995 g, 5.90 mmol) and water (100 mL) under stirring at room temperature. The resultant mixture obtained was stirred at 50 °C for 30 min. After that, the solution was cooled down to room temperature, and an aqueous solution (50 mL) of $\text{Cu}(\text{NO}_3)_2 \cdot 3\text{H}_2\text{O}$ (2.42 g, 5.66 mmol) was added dropwise. The deep-violet solution was filtered on paper and evaporated completely on a rotary evaporator. The polycrystalline precipitate was solved with absolute ethanol and filtered to eliminate the $(n\text{-Bu}_4\text{N})\text{NO}_3$ white powder. The product was recuperated by evaporation on a rotary evaporator and dried under a vacuum in a desiccator (4.20 g, 85%). Anal. Calcd. for $\text{C}_{44}\text{H}_{80}\text{N}_4\text{O}_6\text{Cu}$ (824.69 g mol⁻¹): C 64.08, H 9.78, N 6.79, Cu 7.71%. Found C 64.30, H 9.70, N 6.66, Cu 7.59%. Selected FTIR data (KBr, cm⁻¹): 3010 [$\nu(\text{C-H})$], 2950 [$\nu(\text{C-H})$], 1625 [$\nu(\text{C=O})$], 1480 [$\nu(\text{C=C})$], 1380, 1350 [$\nu(\text{C-N})$], 525 [$\nu(\text{Cu-O})$].

2.2. Synthesis of $\{[\text{Cu}(\text{bpc})_2][\text{Cu}(\text{dmopba})(\text{H}_2\text{O})]\}_2 \cdot 4\text{H}_2\text{O}$ (**1**)

Compound **1** was prepared in mild conditions and at room temperature using an H-shaped tube as follows: $(n\text{-Bu}_4\text{N})_2[\text{Cu}(\text{dmpba})]$ (0.050 g, 0.06 mmol) was introduced in one arm of an H-shaped tube, and $[\text{Cu}(\text{bpc})_2(\text{H}_2\text{O})_2]\text{NO}_3 \cdot 2\text{H}_2\text{O}$ (0.050 g, 0.13 mmol) was deposited in the other one. The tube was carefully filled with water, capped with parafilm on both arms, and maintained at room temperature allowing for the diffusion of the starting materials. X-ray quality blue crystals were formed after three months. Yield: 43% (0.049 g). Anal. Calcd for $\text{C}_{72}\text{H}_{60}\text{Cu}_6\text{N}_{16}\text{O}_{26}$ (1946.63): C, 44.42; H, 3.11; N, 11.51; Cu, 19.59%. Found: C, 44.31; H, 3.08; N, 11.52; Cu, 19.60%. Selected FTIR data (KBr/cm⁻¹): 3450 [$\nu(\text{O-H})$], 3080 [$\nu(\text{C-H})$], 1698 [$\nu(\text{C=O})_{\text{bpc}}$], 1602, 1600 [$\nu(\text{C=O})$], 1344 [$\nu(\text{C-N})$], 1000 [$\delta(\text{C-H})$].

2.3. Crystallographic Data Collection and Refinement

A well-shaped single crystal used for the X-ray diffraction data collection was arbitrarily chosen from the polycrystalline product **1**. The X-ray diffraction measurements were performed on an Oxford-Diffraction GEMINI diffractometer using Graphite-Enhance Source MoK α radiation ($\lambda = 0.71073 \text{ \AA}$). Data integration and scaling of the reflections and analytical absorption corrections were performed with the programs of the CrysAlis suite [47]. The final unit cell parameters were based on fitting all reflection positions. Structure solution through direct methods and refinement based on F2 through a full-matrix least-squares routine was performed using SHELX-2018/3 [48] within the WinGX [49]. The positions of the carbon, oxygen, nitrogen, and copper atoms were unambiguously assigned on consecutive difference Fourier maps. All atoms except hydrogen were refined with anisotropic atomic displacement parameters. According to the riding model, hydrogen atoms were located in different Fourier maps and included as fixed contributions. For organic moieties, C-H = 0.96 Å and Uiso(H) = 1.5 Ueq(C) for methyl groups, and C-H = 0.93 Å and Uiso(H) = 1.2 Ueq(C) for aromatic carbon. The DFIX and DANG SHELXL-2018/3 commands were used for water groups' geometry: O-H = 0.87 Å and H-O-H = 109.4°. Structure analysis and artwork preparation were performed with Mercury software [46]. The crystal data and data collection and refinement details are shown in Table S1. Further information can be found in Table S2 (bond lengths [Å] and angles [°] for **1**) and Table S3 (hydrogen bond lengths [Å] and angles [°] for **1**, where D and A are the donor and acceptor hydrogen atom), respectively; CCDC 2201495 contains the supplementary crystallographic data for this paper. The data can be obtained free of charge from The Cambridge Crystallographic Data Centre via www.ccdc.cam.ac.uk/getstructures (accessed on 25 September 2022).

2.4. Magnetic Measurements

Direct current (dc) magnetic susceptibility and magnetization measurements were performed on crushed single crystals of **1** in the temperature range 2.0–300 K with a Quantum Design SQUID magnetometer and using an applied magnetic field of 500 Oe. The diamagnetic contributions of the sample and sample holder were considered. Diamagnetic corrections of the constituent atoms were estimated according to Pascal tables [50] as $-9.73 \times 10^{-4} \text{ cm}^3 \text{ mol}^{-1}$ (**1**). Corrections for the temperature-independent paramagnetism [$60 \times 10^{-6} \text{ cm}^3 \text{ mol}^{-1}$ per copper(II) ion] and the magnetization of the sample holder were also applied.

3. Results and Discussion

3.1. Synthesis and Characterization of **1**

Complex **1** is obtained using a green solvent such as water and is air-stable in ambient conditions. Elemental analysis confirmed the obtention of the compound of formula $\{[\text{Cu}(\text{bpca})]_2[\text{Cu}(\text{dmopba})(\text{H}_2\text{O})]\}_2 \cdot 4\text{H}_2\text{O}$. The FTIR spectrum for **1** (Figure S1) shows strong C=O stretching vibrations at 1698 and 1602 cm^{-1} , which are characteristic of the carbonyl amide from the $[\text{Cu}(\text{bpca})]^+$ and carbonyl groups from $[\text{Cu}(\text{dmopba})(\text{H}_2\text{O})]^{2-}$ fragments, respectively [51,52]. The TG and DTG curves (Figure S2) show two events that occur from room temperature until 106 °C and refer to the weight loss of 5.37% of the mass of **1**, which can be associated with the loss of approximately six water molecules (calc. 5.54%), being assigned to the four crystallization and two of the coordinated water molecules, in agreement with the formula proposed by elemental analysis. At approximately 350 °C, a third event associated with the decomposition of the ligands occurs.

Experimental and simulated powder X-ray diffraction patterns of **1** (Figure S3) exhibit a significant coincidence between the peaks, confirming the purity of the sample.

3.2. Description of the Crystal Structure of **1**

Compound **1** crystallizes in the triclinic space group $P\bar{1}$ with the asymmetric unit composed of a neutral oxamato-bridged trinuclear copper(II) unit, $\{[\text{Cu}(\text{bpca})]_2[\text{Cu}(\text{dmopba})(\text{H}_2\text{O})]\}$, where the $[\text{Cu}(\text{dmopba})]^{2-}$ anion is coordinated to two $\{[\text{Cu}(\text{bpca})]^+\}$ cations through the oxamato groups together with two water molecules of crystallization (Figure 1a). Two tricopper(II) units are additionally coordinated through the carbonyl oxygen atoms (O2 and O2ⁱ; symmetry code: (i) = $-x + 1, -y + 1, -z + 1$) of the carboxylate portion of one oxamate bridging group, resulting in an overall centrosymmetric linear hexanuclear copper(II) entity with a dimer-of-trinuclear topology (Figure 1b). The coordination polyhedra of the copper atoms in **1** are also depicted in Figure 1b highlighting different geometries: Cu2 and Cu3 exhibit a square pyramidal geometry, whereas Cu1 adopts a distorted octahedral geometry within an edge-sharing octahedral motif environment. The geometry of the three copper(II) ions was also verified through SHAPE measurements software (Table S4) [53]. According to these results, the pentacoordinate Cu2 and Cu3 atoms present a spherical square pyramid (SPY-5) and vacant octahedral symmetry (v-OC), respectively, while the hexacoordinate Cu3 atom exhibits a distorted octahedral (OC) symmetry.

The basal plane of the Cu2 and Cu3 atoms is built by two amidate nitrogen and two carboxylate oxygen atoms from the dmopba ligand (Cu2) or one carbonyl amide oxygen atom from the dmopba ligand and one amidate and two pyridine nitrogen atoms from the bpca ligand (Cu3), while the apical positions are occupied by one oxygen atom from the coordinated water molecule (Cu2) or the carbonyl oxygen atom from the dmopba ligand (Cu3). At the same time, one carbonyl oxygen atom from the carboxylate group of the dmopba ligand and one amidate and two pyridine nitrogen atoms from the bpca ligand form the equatorial plane of the Cu1 atom, while the two axial positions are occupied by two carbonyl oxygen atoms from the amide and carboxylate groups from the dmopba ligands of the two centrosymmetrically related trinuclear units. The Cu2 and Cu3 atoms are almost in the plane formed by their respective basal planes of the square pyramid: Cu2 is shifted from the mean basal plane (r.m.s. deviation of fitted atoms = 0.0039) formed

by N1N2O3O4 atoms by 0.063(1) Å toward the apical position, whereas Cu3 is shifted by 0.106(1) Å from the least-squares plane through N6N7N8C5 (r.m.s = 0.0468). The basal Cu–N and Cu–O distances from the dmopba ligand in the $[\text{Cu}(\text{dmopba})(\text{H}_2\text{O})]^{2-}$ fragment, as well as the basal/equatorial Cu–N distances from the bpca ligand in the $[\text{Cu}(\text{bpca})]^+$ ones, are significantly shorter than the apical Cu–Ow or axial Cu–O distances (see Table S2), being within the ranges found in similar compounds [18,43,52,54]. Within the trinuclear unit, the mean basal plane of the Cu2 atom is perpendicularly oriented to the mean equatorial/basal planes of the Cu1 and Cu3 atoms (78.09 and 81.67°), which in turn have a parallel planar disposition between each other (20.49°).

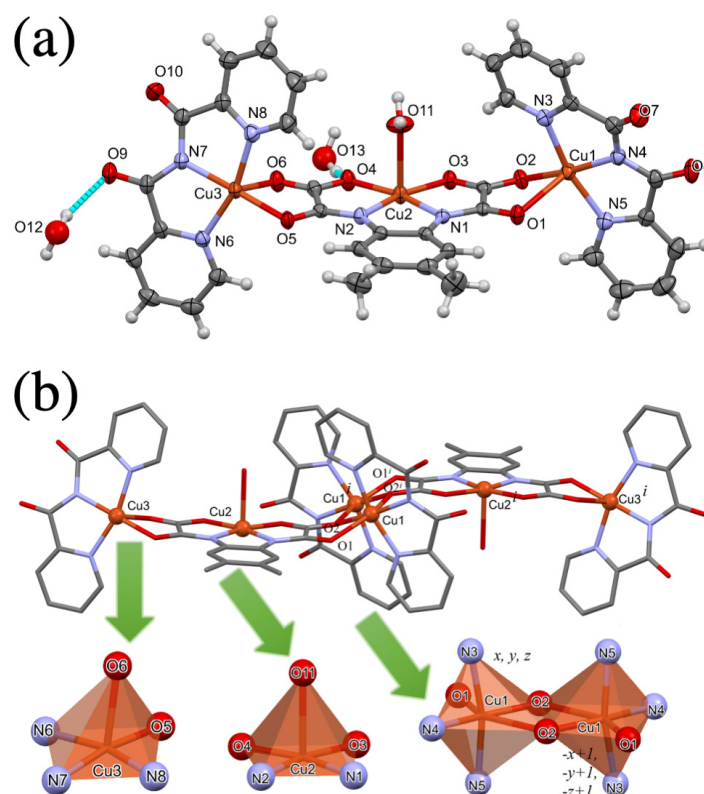


Figure 1. (a) Perspective view of the asymmetric unit of **1** with atom labeling scheme (H bonds involving the water molecules of crystallization are in cyan dotted lines; thermal ellipsoids at 50% probability level); (b) view of the centrosymmetric hexacopper(II) entity of **1** [symmetry code: (i) $-x + 1, -y + 1, -z + 1$] with a detail of the metal coordination polyhedra (hydrogen atoms and crystallization water molecules were hidden for the sake of clarity).

The coordination mode exhibited by the dmopba ligand in the hexanuclear complex is unusual, whereby the two distinct oxamato groups adopt bis(bidentate) ($\mu\text{-}\kappa^2\text{N},\text{O}:\kappa^2\text{O}',\text{O}''$) and bis(bidentate)/monodentate ($\mu_3\text{-}\kappa^2\text{N},\text{O}:\kappa^2\text{O}',\text{O}'':\kappa\text{O}'''$) bridging modes [55].

The dimerization of the trinuclear units (Figure 1b) leads to a copper...copper intertrinuclear separation through the $\mu_3\text{-ox-}\kappa^2\text{N},\text{O}:\kappa^2\text{O}',\text{O}'':\kappa\text{O}'''$: bridge $[\text{Cu}1 \cdots \text{Cu}1^i = 3.685(1)$ Å], which is rather shorter than the intratrinuclear distances across the $\mu_3\text{-ox-}\kappa^2\text{N},\text{O}:\kappa^2\text{O}',\text{O}'':\kappa\text{O}'''$ and $\mu\text{-}\kappa^2\text{N},\text{O}:\kappa^2\text{O}',\text{O}''$: bridges (Cu1·Cu2 = 5.282(1) and Cu2·Cu3 = 5.251(1) Å, respectively). Focusing on the Cu_2O_2 diamond core of the dinuclear entity formed by the $[\text{Cu}(\text{bpca})]^+$ ions, the equatorial and axial Cu1–O2 and Cu1–O2ⁱ distances are 1.969(1) and 2.629(2) Å, respectively, while the θ and φ angles at the bridgehead carboxylate oxygen are equal to $74.37(7)^\circ$ $[\text{O}2\text{-Cu}1\text{-O}2^i]$ and $105.63(8)^\circ$ $[\text{Cu}1\text{-O}2\text{-Cu}1^i]$, respectively (Figure 2a). It adopts a parallel planar “out-of-plane” disposition of the equatorial metal planes. The mean metal equatorial planes are separated by 2.958 Å and orthogonal (85.96°) to the least-squares plane through the bridgehead carboxylate oxygen atoms (Figure 2b).

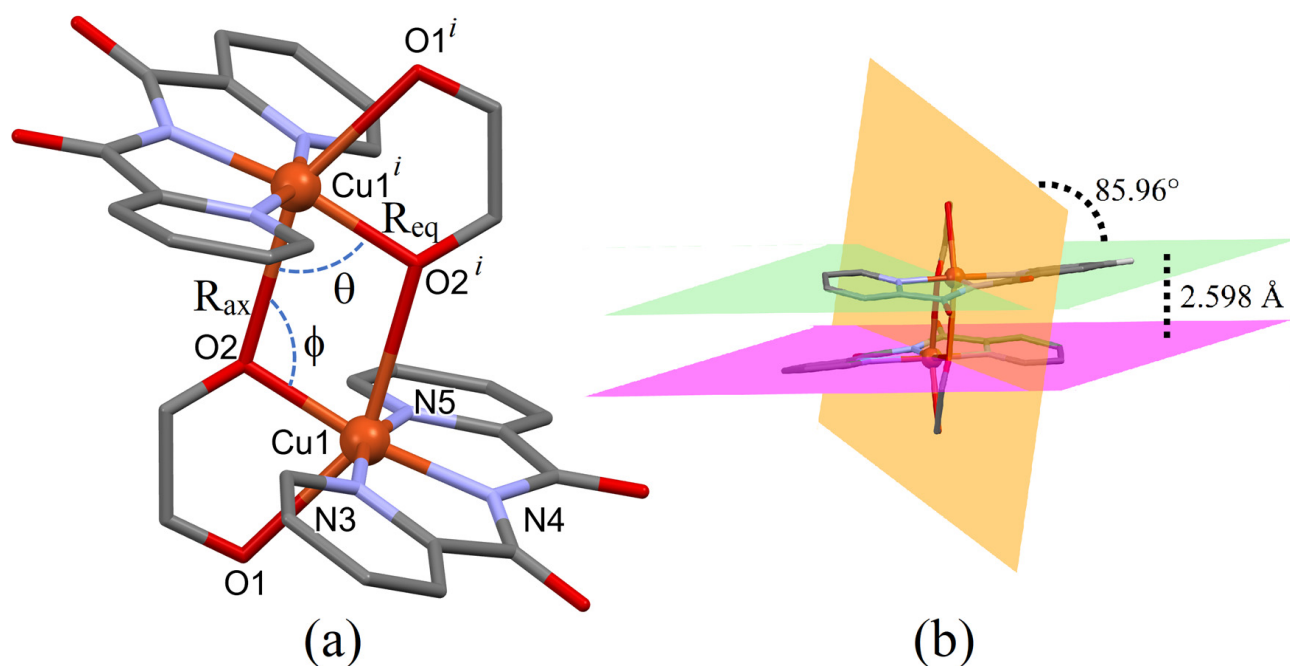


Figure 2. (a) Detail of the double oxo(carboxylate-oxamate)dicopper(II) entity in **1** depicting the equatorial Cu1–O2 [$R_{eq} = 1.969(1) \text{ \AA}$] and axial Cu1–O2ⁱⁱ [$R_{ax} = 2.629(2) \text{ \AA}$] bond distances and the corresponding O2–Cu1–O2ⁱⁱ [$\theta = 74.37(7)^\circ$] and Cu1–O2–Cu1ⁱⁱ [$\phi = 105.63(8)^\circ$] bond angles within the Cu₂O₂ core (b); a view of the mean metal equatorial planes thought the least-squares plane of the bridgedhead carboxylate oxygens. Hydrogen atoms are hidden for the sake of clarity.

In the crystal lattice, the adjacent centrosymmetrically related hexanuclear entities are connected via classical and non-classical H-bonds forming infinite chains along the [011] direction (Figure 3a). The oxygen atom (O11) from the coordinate water molecule of the [Cu(dmopba)]²⁻ unit works as an H bond donor to one of the carboxylate oxygen atoms (O10) of the [Cu(bpca)]⁺ unit [O11–H112...O10ⁱⁱ; symmetry code: (ii) = $-x + 1, -y + 2, -z + 2$]. The non-classical H bonds involve two aromatic carbon atoms from both bpca ligands [C14–H14...O10ⁱⁱ and C34ⁱⁱ–H34ⁱⁱ...O6]. The chains are themselves connected through H bonds along the [100] direction (Figure 3b), being stabilized by one classical H bond involving the coordinate water molecule atom [O11–H111...O7ⁱⁱⁱ; symmetry code: (iii) = $-x, -y + 1, -z + 1$] and three non-classical H bonds involving the aromatic carbons from the bpca ligands, C15ⁱⁱⁱ–H15ⁱⁱⁱ...O1, C35–H35...O8ⁱⁱⁱ, and C35–H35...O7ⁱⁱⁱ. The resulting 2D H bond network is stacked along the [0 $\bar{1}$ 1] direction (Figure 3c). The H bond geometries are given in Table S3 (Supplementary Materials).

The two crystallization water molecules form centrosymmetric tetrameric clusters stabilized by H bonds positioned at the unit cell corners (Figure S4a). The voids occupied by the water molecules calculated through the Mercury software using the contact surface approach with grid spacing and a probing sphere radius of 0.7 and 1.1 \AA , respectively, present an accessible void volume of 121.39 \AA^3 , which corresponds to 6.6% of all unit cell volume (Figure S4b). Therefore, the water molecules are essential to the crystal packing stabilization. Each water cluster is surrounded by four hexanuclear units interacting via H bonds (Figure S4c). The H bond geometries are given in Table S3 (Supplementary Materials).

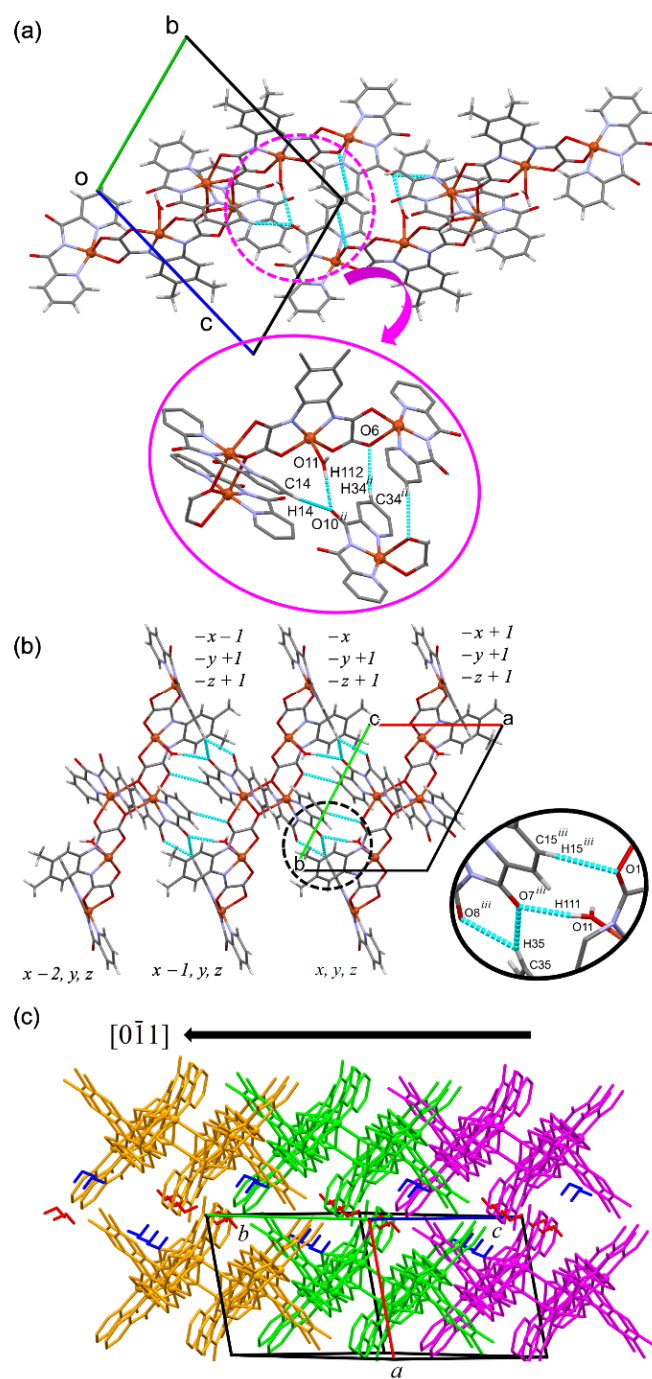


Figure 3. Partial view of the crystal packing of **1** along the crystallographic [011] (a) and [100] directions (b) showing the supramolecular connections of the hexanuclear units via hydrogen bonds (dashed cyan lines). The resulting 3D supramolecular coordination network (c) highlights the layered structure staked along the $[0\bar{1}1]$ direction (each color is a layer). Symmetry codes: (ii) $-x + 1, -y + 2, -z + 2$; (iii) $-x, -y + 1, -z + 1$. Hydrogen atoms were omitted in some views for clarity.

The packing is also stabilized by π - π stacking interactions involving bpca and dmopba ligands (Figure 4), which are responsible for the closest interhexanuclear unit Cu·Cu separations: $[\text{Cu}2\cdot\text{Cu}2^{\text{vi}} = 5.648 \text{ \AA}$ and $\text{Cu}1\cdot\text{Cu}2^{\text{vi}} = 5.969 \text{ \AA}$; symmetry code: (vi) = (vi) = $-x + 1, -y + 2, -z + 1$). A stair-like chain is formed along the crystallographic b axis with two step-rises of 3.255 and 1.110 \AA (Figure S5). Parallel chains along the crystallographic c axis enable Cu·Cu separations in the range from 7.883 \AA ($\text{Cu}3\cdot\text{Cu}3^{\text{vi}}$) to 8.355 \AA ($\text{Cu}2\cdot\text{Cu}3^{\text{ii}}$) (symmetry code: (ii) $-x + 1, -y + 2, -z + 2$; (vii) = $-x + 1, -y + 3, -z + 2$).

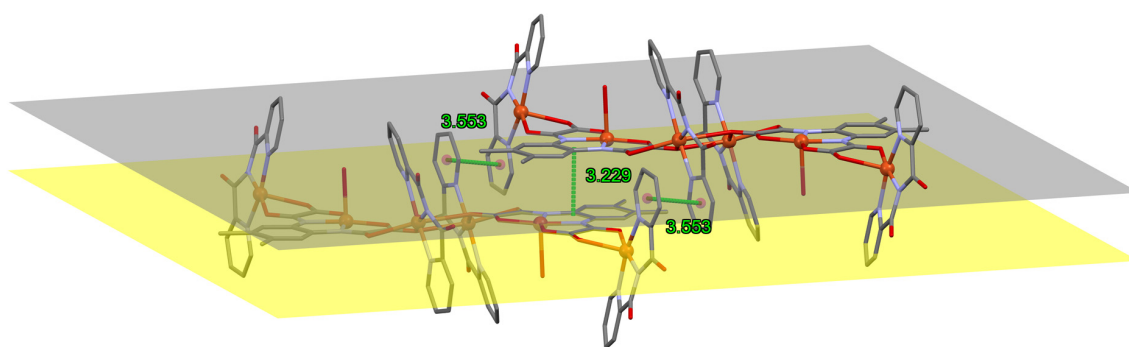


Figure 4. Centrosymmetrically related pair of hexanuclear units highlighting the π - π stacking involving bpca and dmopba ligands. The centroid distance (3.553 Å) between the closest bpca pyridyl rings, as well as the distance (3.229 Å) between the least-squares plane through the closest $[\text{Cu}(\text{dmopba})(\text{H}_2\text{O})]^{2-}$ moieties (in gray and yellow) are depicted as dashed green lines. Hydrogen atoms were omitted for clarity.

3.3. Magnetic Properties of **1**

The magnetic properties of **1** in the form of the $\chi_M T$ versus T plot (χ_M is the magnetic susceptibility per six copper(II) ions, and T is the temperature) are shown in Figure 5. At room temperature, the $\chi_M T$ value of $2.18 \text{ cm}^3 \text{ K mol}^{-1}$ is slightly below the expected value for six magnetically isolated copper(II) ions ($2.25 \text{ cm}^3 \text{ K mol}^{-1}$, with $S_{\text{Cu}} = 1/2$ and $g_{\text{Cu}} = 2.0$). Since the obtained value is slightly below the expected one, it can occur due to the presence of antiferromagnetic interactions in **1** at room temperature. Upon cooling, the $\chi_M T$ decreases continuously, probably due to the antiferromagnetic interactions inside each trinuclear unit, until it reaches a plateau in the temperature region of around 10–20 K, reaching a $\chi_M T$ value of $0.87 \text{ cm}^3 \text{ K mol}^{-1}$. This value agrees with two trinuclear units with an $S = 1/2$ ground state ($0.80 \text{ cm}^3 \text{ K mol}^{-1}$, with $g = 2.0$). Below this temperature, the $\chi_M T$ product shows a slight increase, reaching the value of $0.90 \text{ cm}^3 \text{ K mol}^{-1}$ at 5 K, suggesting the occurrence of weak ferromagnetic coupling between the two trinuclear units.

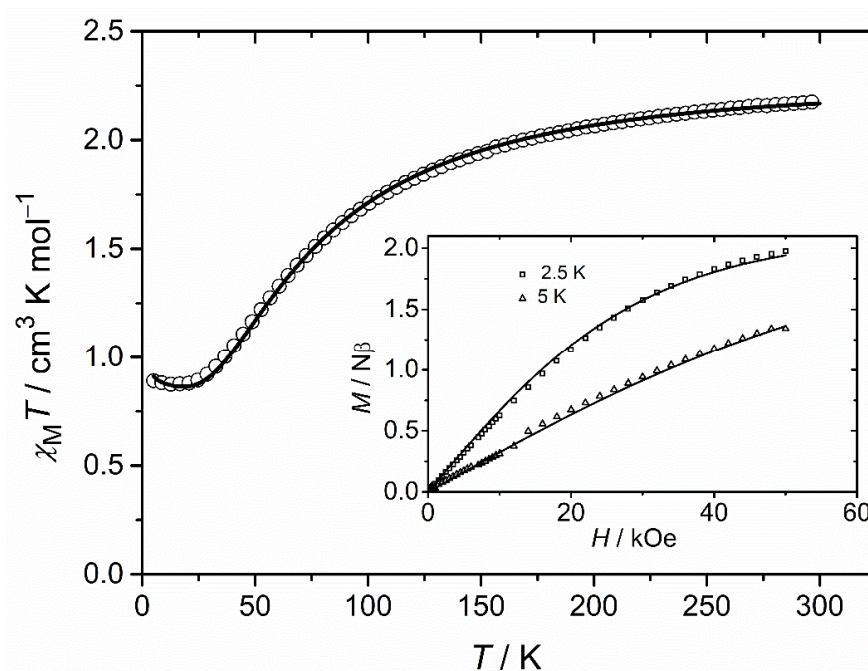
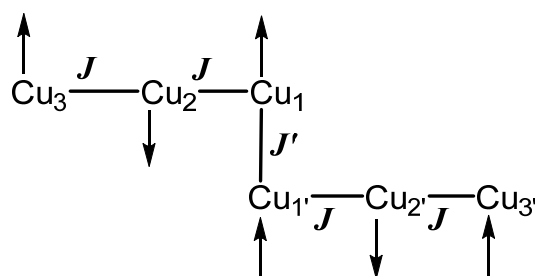


Figure 5. $\chi_M T$ versus T curve for **1** ($H = 0.5 \text{ kOe}$). Inset: M versus H curves measured at 2.5 and 5 K. The solid lines represent the best-fit curves (see text).

The experimental magnetic data were analyzed using the spin Hamiltonian given by Equation (1) (with $S_1 = S_2 = S_3 = S_{1'} = S_{2'} = S_{3'} = 1/2$), where J ($J = J_{12} = J_{23} = J_{1'2'} = J_{2'3'}$) and J' ($J' = J_{11'}$) are the intra- and intertrinuclear magnetic coupling parameters (Scheme 2), and g is the average Landé factor of the copper(II) ions ($g = g_1 = g_2 = g_3 = g_{1'} = g_{2'} = g_{3'}$). The $\chi_M T$ versus T and M versus H curves were fitted simultaneously using the PHI software (version 3.1.6, N. Chilton, Manchester, UK) [56], resulting in the following parameters: $J = -31.96(2) \text{ cm}^{-1}$; $J' = +1.34(2) \text{ cm}^{-1}$; and $g = 2.12(1)$ with $R_{(\chi T)} = 2.21 \times 10^{-5}$, $R_{(M \times H \text{ 2.5K})} = 5.32 \times 10^{-4}$ and $R_{(M \times H \text{ 5K})} = 9.95 \times 10^{-4}$ (R is the agreement factor defined as $R = \sum [P_{\text{exp}} - P_{\text{calcd}}]^2 / \sum (P_{\text{exp}})^2$, with P being the measured physical property). The theoretical curves match perfectly with the experimental data (Figure 5).

$$H = J (S_1 \cdot S_2 + S_2 \cdot S_3 + S_{1'} \cdot S_{2'} + S_{2'} \cdot S_{3'}) + J' (S_1 \cdot S_{1'}) + g\beta H (S_1 + S_2 + S_3 + S_{1'} + S_{2'} + S_{3'}) \quad (1)$$



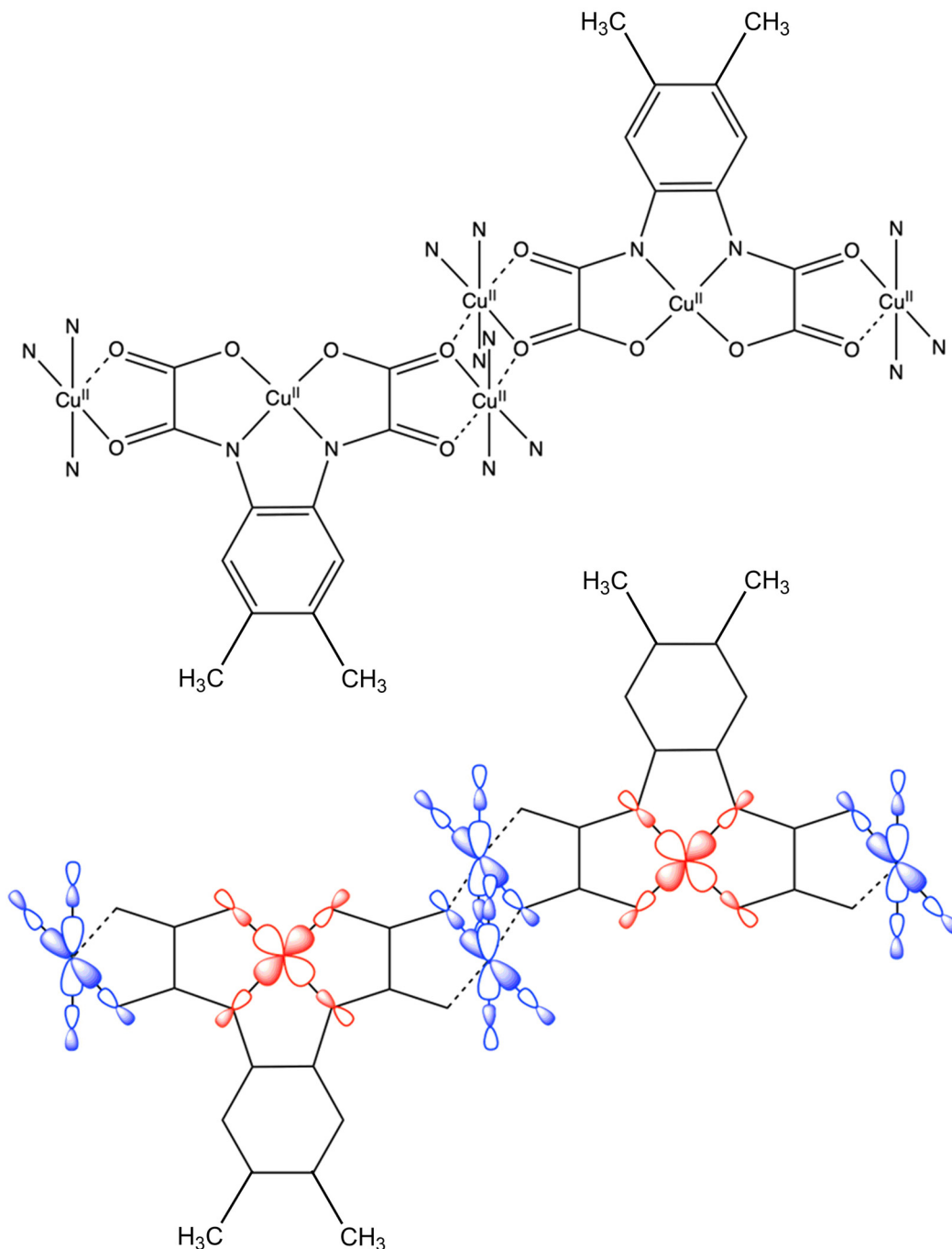
Scheme 2. Exchange coupling model in **1**.

The moderate intratrinuclear antiferromagnetic coupling through the oxamato bridge observed for **1** ($J = -31.96 \text{ cm}^{-1}$) is an order of magnitude smaller than that found for trinuclear compounds with bidentate blocking ligands ($\sim -350 \text{ cm}^{-1}$), comparable to that found for tri- and hexanuclear compounds with tridentate blocking ligands ($\sim -84 \text{ cm}^{-1}$) [18,36]. It is well known that the strength of magnetic coupling is directly linked to the symmetry and relative orientation of the magnetic orbitals involved, which ultimately depend on the geometry of the metal ions and the nature of the blocking ligands [57].

The presence of an extensive hydrogen bond network suggests their participation in the magnetic properties [37–39]. The possible interactions between the trinuclear entities can be observed in Figure 4 and Table S3. Differently from what was observed in the structures reported previously [37–39], in the case of **1**, most of them present a large distance between the metal ions. Consequently, there are many atoms involved in this pathway since they use water molecules of crystallization, in which they are not firmly bound to the metal ions. The exception occurs in the case of the water molecule coordinated to Cu2, which connects this metal to the amide oxygen of the bpca ligand and consequently to Cu3ⁱⁱ (Cu2–O11–H112...O10–C32–N7–Cu3ⁱⁱ). A similar pathway is observed in the same Cu2 atom but leading to C1ⁱⁱ (Cu2–O11–H111...O7–C19–N4–Cu1ⁱⁱ). Even through covalent bonds, these pathways are considered very distant (8.4 Å and 8.57 Å for Cu2–Cu3ⁱⁱ and Cu2–C1ⁱⁱ, respectively). In comparison with the compounds $[\{\text{Cu}(\text{H}_2\text{O})(\text{tmen})\text{Cu}(\text{tmen})\}\{\mu\text{-Cu}(\text{H}_2\text{O})(\text{Me}_2\text{pba})\}]_n(\text{PF}_6)_2 \cdot 2n\text{H}_2\text{O}$, $[\{\text{Cu}(\text{H}_2\text{O})(\text{tmen})\text{Cu}(\text{NCS})(\text{tmen})\}\{\mu\text{-Cu}(\text{H}_2\text{O})(\text{Me}_2\text{pba})\}]_2(\text{ClO}_4)_2 \cdot 4\text{H}_2\text{O}$, and $[\{\text{Cu}(\text{H}_2\text{O})(\text{tmen})\text{Cu}(\text{NCS})(\text{tmen})\}\{\mu\text{-Cu}(\text{H}_2\text{O})(\text{Me}_2\text{pba})\}]_2(\text{PF}_6)_2 \cdot 4\text{H}_2\text{O}$ (**3**), where Me₂pba = 2,2-dimethyl-1,3-propylenebis(oxamato) and tmen = *N,N,N',N'*-tetramethylethylenediamine [39], the Cu...Cu intermolecular distances are 6.1 Å smaller on average. These lower values are explained by the pathway formed involving fewer atoms, which generally involves hydrogen bonds formed between water molecules coordinated directly on copper(II) ions, as occurs in other examples [37–39]. Therefore, due to the longest distances between the copper(II) ions and the hexanuclear entities in **1**, the possible magnetic interactions between trinuclear species considering the interactions through these pathways can be disregarded.

In **1**, the geometry of the Cu2 atom (= 0.003) is square pyramidal (SPY), while Cu3 (= 0.110) presents a small distortion of the SPY symmetry toward trigonal bipyramidal (TBP), as expressed by the values of the trigonality parameter (= 0 and 1 for ideal SPY

and TBP geometries, respectively) [58]. Moreover, the basal planes of the three copper(II) ions are not coplanar. This fact makes the orientation of the $d_{x^2-y^2}$ magnetic orbitals, aiming at an overlap, unfavorable, which strongly contributes to a drastic decrease in the strength of the observed antiferromagnetic coupling, as illustrated in Scheme 3.



Scheme 3. Illustration of the orbital exchange pathway in **1** showing the nature and orientation of the magnetic orbitals of the copper(II) ions. The bpca blocking ligands are not shown for clarity. The solid and dashed lines represent short and long metal–ligand bonds.

The intratrinnuclear magnetic coupling of **1** can be estimated by an earlier magneto-structural correlation found for related trinuclear copper(II) oxamate complexes with similar geometries [36]. In such an approximation, we can assume that the Cu1 atom is pentacoordinate, and the estimative of the τ value is 0.10. Considering that the τ value is 0.12 for the Cu3 atom, we can estimate an average value for τ equal to 0.11 for the terminal

copper(II) ions in the trinuclear unit of **1**. From the proposed linear relationship between the J and τ values [36], we can obtain an estimated J value of around -40 cm^{-1} for **1**. This value is close to the experimental one (-31.96 cm^{-1}) obtained through the best fit curve. This difference in these values can be attributed to the fact that Cu1 and Cu1ⁱ do not have the square pyramidal geometry. Additionally, a few examples of “dimer-of-trinuclear” or “chain-of-trinuclear” complexes are described in the literature involving the parent unsubstituted 1,2-phenylenebis(oxamate) (opba) and related 1,3-propylenebis(oxamate) (pba) derivatives depending on the nature of the terminal blocking ligand coordinated to copper(II) ions [36–39]. In these latter cases, the supramolecular aggregation process occurs through weak intermolecular π – π stacking or hydrogen bonding interactions in the solid state which lead to a global intertrinuclear antiferromagnetic interaction, instead of the intertrinuclear ferromagnetic one found in **1** across the weak coordinative interactions.

Finally, to describe the weak ferromagnetic interaction between the two trinuclear moieties in **1**, we need to consider the hexanuclear structure once there is an orbital pathway between Cu1 and Cu1ⁱ atoms from two [Cu(bpca)]⁺ cations through the carbonyl carboxylate oxygen atoms of the oxamate bridge, as illustrated in Scheme 3. Focusing on the Cu₂O₂ bridging core, **1** could exhibit intertrinuclear ferromagnetic or antiferromagnetic couplings. The main structural feature that contributes to the determination of the kind of magnetic coupling is the Cu–O–Cu angle, which is related to the combination of the $d_{x^2-y^2}$ magnetic orbitals of the copper(II) ions with the symmetry-adapted molecular orbitals of the oxamate bridge [39,59]. As reported elsewhere [59], an antiferromagnetic character is found for dicopper(II) compounds with an out-of-plane parallel planar disposition in which this angle is more significant than 95.34° . Likewise, ferromagnetic behavior appeared in compounds in which this value is higher than 101.9° . In **1**, the Cu–O–Cu angle is $105.63(8)^\circ$ (Figure 2a), supporting the ferromagnetic behavior ($J' = +1.39\text{ cm}^{-1}$). This value agrees with some results reported for distorted octahedral carboxylate bridged Cu₂O₂ units described in the literature [59–63].

4. Conclusions

In this work, we present a novel homohexanuclear compound containing oxamate ligands and copper(II) atoms obtained at room temperature and in ambient conditions, being air stable. The synthesis method used to produce this compound was the slow diffusion through an H-shaped tube and water as a solvent. We believe that the choice of this synthesis method is crucial to obtaining this unique copper(II) oxamate structure once the reaction occurs very slowly, which can permit the nucleation and growth of the hexanuclear compound.

The crystal structure comprises two oxamato-bridged trinuclear copper(II) units connected through carbonyl carboxylate oxygen atoms from the oxamato groups leading to a Cu₂O₂ bridging core. An important feature of this structure is the presence of copper(II) ions with different geometries, four of them approximately square pyramidal. In contrast, the other two are elongated octahedral according to the Jahn Teller effect.

The magnetic properties were evaluated, and the fit of the experimental data showed that **1** presents a weak antiferromagnetic interaction ($J = -31.96\text{ cm}^{-1}$) in the trinuclear unit in comparison to other oxamato-bridged trinuclear copper(II) complexes, due to the lack of planarity between the three copper(II) ions of each trinuclear entity. A weak ferromagnetic coupling ($J' = +1.34\text{ cm}^{-1}$) is also observed between two trinuclear entities through the Cu₂O₂ bridging core, leading to a rare example of a homometallic hexanuclear copper(II) oxamate complex with alternating antiferro- and ferromagnetic couplings. The rational design and fabrication of polynuclear complexes with predetermined structures and predictable properties is still a challenge in metallosupramolecular chemistry and molecular magnetism. Thus, further studies to obtain this product and others using different synthetic approaches from that in the present work will be carried out to shed light on the supramolecular self-assembly of synthetic magnetic nanostructures with potential technological applications.

Supplementary Materials: The following supporting information can be downloaded at: <https://www.mdpi.com/article/10.3390/magnetochemistry8100116/s1>, Figure S1: FTIR spectrum of **1**; Figure S2: TG (solid line) and DTG (dashed line) curves for **1** in N_{2(g)} atmosphere; Figure S3: Experimental (solid black line) and simulated (solid red line) PXRD patterns for **1**; Figure S4: (a) View the crystallization water super-structure depicting the tetramer-cluster at the unit cell corner and (b) the calculated voids (surfaces in orange) surrounding a hexanuclear unit inside the unit cell in the same perspective view. View of each water-cluster surrounded by four hexanuclear units (c) being stabilized by the H bond network. The scheme color (red and blue) in (a) differentiates the independent symmetry of water molecules in the asymmetric unit. H bond is in dashed cyan lines. Non-water hydrogen atoms were omitted in some views for clarity; Figure S5: (a) Packing view of the hexanuclear units showing the chains along the crystallographic *b* axis showing the shortest interhexanuclear Cu...Cu distances (dashed green lines). (b) The perspective view of the star-like chain showing the parallel disposition of the hexanuclear units along the crystallographic *c* axis is shifted along the crystallographic *b* axis resulting in a stair-like chain formed along the crystallographic *b* axis with two-step rises (highlighted in magenta dashed lines). Just the copper atoms and part of the dmopba ligand were used to generate the illustration for clarity. Table S1: Crystal data and structure refinement for **1**; Table S2: Bond lengths [Å] and angles [°] for **1**; Table S3: Hydrogen bond lengths [Å] and angles [°] for **1**, where D and A are the donor and acceptor hydrogen atom, respectively; Table S4. Shape measurements analysis for **1***.

Author Contributions: A.L.A.L. and L.A.R. performed the synthesis and experimental characterization; A.C.D. solved the crystal structure and interpretation; C.B.P. measured the X-ray pattern; E.F.P., W.C.N. and E.F.P. carried out the magnetic measurements and interpretation; C.L.M.P. guided the students, supervised all the experiments, and was responsible for funding acquisition. A.C.D. and C.L.M.P. wrote this paper. All authors have read and agreed to the published version of the manuscript.

Funding: This work was supported by Conselho Nacional de Desenvolvimento Científico e Tecnológico (CNPq), Projects 309874/2021-1 and 308893/2019-0, Fundação de Amparo à Pesquisa do Estado de Minas Gerais (FAPEMIG), PPM 00630-18, Coordenação de Aperfeiçoamento de Pessoal de Nível Superior (CAPES), Finance code 001, Fundação de Amparo à Pesquisa do Estado do Rio de Janeiro (FAPERJ), Projects E-26/010.000978/2019 and E-26/010.1553/2019). Additionally, authors acknowledge the BioAnalytical Facility NEPS-DQ (<https://ne.qui.ufmg.br>, accessed on 26 September 2022) at Universidade Federal de Minas Gerais for their support in chemical analysis.

Conflicts of Interest: The authors declare no conflict of interest.

References

1. Mako, T.L.; Racicot, J.M.; Levine, M. Supramolecular Luminescent Sensors. *Chem. Rev.* **2019**, *119*, 322–477. [[CrossRef](#)]
2. Tang, Y.-Y.; Zeng, Y.-L.; Xiong, R.-G. Contactless Manipulation of Write–Read–Erase Data Storage in Diarylethene Ferroelectric Crystals. *J. Am. Chem. Soc.* **2022**, *144*, 8633–8640. [[CrossRef](#)]
3. Olivo, G.; Capocasa, G.; del Giudice, D.; Lanzalunga, O.; di Stefano, S. New Horizons for Catalysis Disclosed by Supramolecular Chemistry. *Chem. Soc. Rev.* **2021**, *50*, 7681–7724. [[CrossRef](#)]
4. Chen, Y.; Huang, Z.; Zhao, H.; Xu, J.-F.; Sun, Z.; Zhang, X. Supramolecular Chemotherapy: Cooperative Enhancement of Antitumor Activity by Combining Controlled Release of Oxaliplatin and Consuming of Spermine by Cucurbit[7]Uril. *ACS Appl. Mater. Interfaces* **2017**, *9*, 8602–8608. [[CrossRef](#)]
5. Dumele, O.; Chen, J.; Passarelli, J.v.; Stupp, S.I. Supramolecular Energy Materials. *Adv. Mater.* **2020**, *32*, 1907247. [[CrossRef](#)]
6. Irie, M.; Fukaminato, T.; Matsuda, K.; Kobatake, S. Photochromism of Diarylethene Molecules and Crystals: Memories, Switches, and Actuators. *Chem. Rev.* **2014**, *114*, 12174–12277. [[CrossRef](#)]
7. Geng, W.; Zheng, Z.; Guo, D. Supramolecular Design Based Activatable Magnetic Resonance Imaging. *View* **2021**, *2*, 20200059. [[CrossRef](#)]
8. Moreno-Pineda, E.; Wernsdorfer, W. Measuring Molecular Magnets for Quantum Technologies. *Nat. Rev. Phys.* **2021**, *3*, 645–659. [[CrossRef](#)]
9. Fyfe, M.C.T.; Stoddart, J.F. Synthetic Supramolecular Chemistry. *Acc. Chem. Res.* **1997**, *30*, 393–401. [[CrossRef](#)]
10. Dhers, S.; Feltham, H.L.C.; Brooker, S. A Toolbox of Building Blocks, Linkers and Crystallisation Methods Used to Generate Single-Chain Magnets. *Coord. Chem. Rev.* **2015**, *296*, 24–44. [[CrossRef](#)]
11. Journaux, Y.; Ferrando-Soria, J.; Pardo, E.; Ruiz-Garcia, R.; Julve, M.; Lloret, F.; Cano, J.; Li, Y.; Lisnard, L.; Yu, P.; et al. Design of Magnetic Coordination Polymers Built from Polyoxalamide Ligands: A Thirty Year Story. *Eur. J. Inorg. Chem.* **2018**, *2018*, 228–247. [[CrossRef](#)]

12. Dul, M.-C.; Pardo, E.; Lescouëzec, R.; Journaux, Y.; Ferrando-Soria, J.; Ruiz-García, R.; Cano, J.; Julve, M.; Lloret, F.; Cangussu, D.; et al. Supramolecular Coordination Chemistry of Aromatic Polyoxalamide Ligands: A Metallosupramolecular Approach toward Functional Magnetic Materials. *Coord. Chem. Rev.* **2010**, *254*, 2281–2296. [[CrossRef](#)]
13. Ferrando-Soria, J.; Vallejo, J.; Castellano, M.; Martínez-Lillo, J.; Pardo, E.; Cano, J.; Castro, I.; Lloret, F.; Ruiz-García, R.; Julve, M. Molecular Magnetism, Quo Vadis? A Historical Perspective from a Coordination Chemist Viewpoint. *Coord. Chem. Rev.* **2017**, *339*, 17–103. [[CrossRef](#)]
14. Da Cunha, T.T.; da Silveira, C.O.C.; Barbosa, V.M.M.; Oliveira, W.X.C.; da Silva Júnior, E.N.; Ferreira, F.F.; Pedroso, E.F.; Pereira, C.L.M. Ferromagnetic Coupling in a Dicopper(II) Oxamate Complex Bridged by Carboxylate Groups. *CrystEngComm* **2021**, *23*, 1885–1897. [[CrossRef](#)]
15. Da Cunha, T.T.; Barbosa, V.M.M.; Oliveira, W.X.C.; Pedroso, E.F.; García, D.M.A.; Nunes, W.C.; Pereira, C.L.M. Field-Induced Slow Magnetic Relaxation of a Six-Coordinate Mononuclear Manganese(II) and Cobalt(II) Oxamate Complexes. *Inorg. Chem.* **2020**, *59*, 12983–12987. [[CrossRef](#)]
16. Da Cunha, T.T.; Barbosa, V.M.M.; Oliveira, W.X.C.; Pinheiro, C.B.; Pedroso, E.F.; Nunes, W.C.; Pereira, C.L.M. Slow Magnetic Relaxation in Mononuclear Gadolinium(III) and Dysprosium(III) Oxamate Complexes. *Polyhedron* **2019**, *169*, 102–113. [[CrossRef](#)]
17. Do Pim, W.D.; Oliveira, W.X.C.; Ribeiro, M.A.; de Faria, É.N.; Teixeira, I.F.; Stumpf, H.O.; Lago, R.M.; Pereira, C.L.M.; Pinheiro, C.B.; Figueiredo-Júnior, J.C.D.; et al. A PH-Triggered Bistable Copper(I) Metallacycle as a Reversible Emulsion Switch for Biphasic Processes. *Chem. Commun.* **2013**, *49*, 10778–10780. [[CrossRef](#)]
18. Barros, W.P.; da Silva, B.C.; Reis, N.V.; Pereira, C.L.M.; Doriguetto, A.C.; Cano, J.; Pirola, K.R.; Pedroso, E.F.; Julve, M.; Stumpf, H.O. Discrete Trinuclear Copper(II) Compounds as Building Blocks: The Influence of the Peripheral Substituents on the Magnetic Coupling in Oxamate-Bridged Complexes. *Dalton Trans.* **2014**, *43*, 14586–14595. [[CrossRef](#)]
19. Do Pim, W.D.; de Faria, É.N.; Oliveira, W.X.C.; Pinheiro, C.B.; Nunes, W.C.; Cano, J.; Lloret, F.; Julve, M.; Stumpf, H.O.; Pereira, C.L.M. A Heterobimetallic [Mn^{II}₅Cu^{II}₅] Nanowheel Modulated by a Flexible Bis-Oxamate Type Ligand. *Dalton Trans.* **2015**, *44*, 10939–10942. [[CrossRef](#)]
20. Do Pim, W.D.; Silva, I.F.; da Silva Júnior, E.N.; Stumpf, H.O.; Oliveira, W.X.C.; Pedroso, E.F.; Pinheiro, C.B.; Journaux, Y.; Fantuzzi, F.; Krummenacher, I.; et al. Unexpected Formation of a Dodecanuclear {Co^{II}₆Cu^{II}₆} Nanowheel under Ambient Conditions: Magneto-Structural Correlations. *Dalton Trans.* **2021**, *50*, 12430–12434. [[CrossRef](#)]
21. Da Cunha, T.; Oliveira, W.X.C.; Pedroso, E.F.; Lloret, F.; Julve, M.; Pereira, C.L.M. Heterobimetallic One-Dimensional Coordination Polymers MICuII (M = Li and K) Based on Ferromagnetically Coupled Di- and Tetracopper(II) Metallacyclophanes. *Magnetochemistry* **2018**, *4*, 38. [[CrossRef](#)]
22. Marinho, M.V.; Simões, T.R.G.; Ribeiro, M.A.; Pereira, C.L.M.; Machado, F.C.; Pinheiro, C.B.; Stumpf, H.O.; Cano, J.; Lloret, F.; Julve, M. A Two-Dimensional Oxamate- and Oxalate-Bridged Cu^{II}Mn^{II} Motif: Crystal Structure and Magnetic Properties of (Bu₄N)₂[Mn₂{Cu(opba)}₂ox]. *Inorg. Chem.* **2013**, *52*, 8812–8819. [[CrossRef](#)]
23. Pardo, E.; Cangussu, D.; Dul, M.-C.; Lescouëzec, R.; Herson, P.; Journaux, Y.; Pedroso, E.F.; Pereira, C.L.M.; Muñoz, M.C.; Ruiz-García, R.; et al. A Metallacryptand-Based Manganese(II)-Cobalt(II) Ferrimagnet with a Three-Dimensional Honeycomb Open-Framework Architecture. *Angew. Chem. Int. Ed.* **2008**, *47*, 4279–4284. [[CrossRef](#)]
24. Viciano-Chumillas, M.; Mon, M.; Ferrando-Soria, J.; Corma, A.; Leyva-Pérez, A.; Armentano, D.; Pardo, E. Metal–Organic Frameworks as Chemical Nanoreactors: Synthesis and Stabilization of Catalytically Active Metal Species in Confined Spaces. *Acc. Chem. Res.* **2020**, *53*, 520–531. [[CrossRef](#)]
25. Desiraju, G.R. Chemistry beyond the Molecule. *Nature* **2001**, *412*, 397–400. [[CrossRef](#)] [[PubMed](#)]
26. Lehn, J.-M. Perspectives in Chemistry—Steps towards Complex Matter. *Angew. Chem. Int. Ed.* **2013**, *52*, 2836–2850. [[CrossRef](#)]
27. Oliveira, W.X.C.; da Costa, M.M.; Fontes, A.P.S.; Pinheiro, C.B.; de Paula, F.C.S.; Jaimes, E.H.L.; Pedroso, E.F.; de Souza, P.P.; Pereira-Maia, E.C.; Pereira, C.L.M. Palladium(II) and Platinum(II) Oxamate Complexes as Potential Anticancer Agents: Structural Characterization and Cytotoxic Activity. *Polyhedron* **2014**, *76*, 16–21. [[CrossRef](#)]
28. Kovač, V.; Kodrin, I.; Radošević, K.; Molčanov, K.; Adhikari, B.; Kraatz, H.-B.; Barišić, L. Oxalamide-Bridged Ferrocenes: Conformational and Gelation Properties and *In Vitro* Antitumor Activity. *Organometallics* **2022**, *41*, 920–936. [[CrossRef](#)]
29. Altinoz, M.A.; Ozpinar, A. Oxamate Targeting Aggressive Cancers with Special Emphasis to Brain Tumors. *Biomed. Pharmacother.* **2022**, *147*, 112686. [[CrossRef](#)]
30. Fortea-Pérez, F.R.; Armentano, D.; Julve, M.; de Munno, G.; Stiriba, S.E. Bis(Oxamate)Palladate(II) Complexes: Synthesis, Crystal Structure and Application to Catalytic Suzuki Reaction. *J. Coord. Chem.* **2014**, *67*, 4003–4015. [[CrossRef](#)]
31. Da Cunha, T.T.; de Souza, T.E.; do Pim, W.D.; de Almeida, L.D.; do Nascimento, G.M.; García-España, E.; Inclán, M.; Julve, M.; Stumpf, H.O.; Oliveira, L.C.A.; et al. A Hybrid Catalyst for Decontamination of Organic Pollutants Based on a Bifunctional Dicopper(II) Complex Anchored over Niobium Oxyhydroxide. *Appl. Catal. B* **2017**, *209*, 339–345. [[CrossRef](#)]
32. Ferrando-Soria, J.; Serra-Crespo, P.; de Lange, M.; Gascon, J.; Kaptejn, F.; Julve, M.; Cano, J.; Lloret, F.; Pasán, J.; Ruiz-Pérez, C.; et al. Selective Gas and Vapor Sorption and Magnetic Sensing by an Isoreticular Mixed-Metal-Organic Framework. *J. Am. Chem. Soc.* **2012**, *134*, 15301–15304. [[CrossRef](#)] [[PubMed](#)]
33. Silva, I.F.; Teixeira, I.F.; Barros, W.P.; Pinheiro, C.B.; Ardisson, J.D.; do Nascimento, G.M.; Pradie, N.A.; Teixeira, A.P.C.; Stumpf, H.O. An Fe^{III} Dinuclear Metallacycle Complex as a Size-Selective Adsorbent for Nitrogenous Compounds and a Potentially Effective Ammonia Storage Material. *J. Mater. Chem. A Mater.* **2019**, *7*, 15225–15232. [[CrossRef](#)]

34. Ferrando-Soria, J.; Khajavi, H.; Serra-Crespo, P.; Gascon, J.; Kapteijn, F.; Julve, M.; Lloret, F.; Pasán, J.; Ruiz-Pérez, C.; Journaux, Y.; et al. Highly Selective Chemical Sensing in a Luminescent Nanoporous Magnet. *Adv. Mater.* **2012**, *24*, 5625–5629. [[CrossRef](#)] [[PubMed](#)]
35. Vaz, R.C.A.; Esteves, I.O.; Oliveira, W.X.C.; Honorato, J.; Martins, F.T.; Marques, L.F.; dos Santos, G.L.; Freire, R.O.; Jesus, L.T.; Pedroso, E.F.; et al. Mononuclear Lanthanide(III)-Oxamate Complexes as New Photoluminescent Field-Induced Single-Molecule Magnets: Solid-State Photophysical and Magnetic Properties. *Dalton Trans.* **2020**, *49*, 16106–16124. [[CrossRef](#)]
36. Costa, R.; Garcia, A.; Ribas, J.; Mallah, T.; Journaux, Y.; Sletten, J.; Solans, X.; Rodriguez, V. Tailored Magnetic Properties in Trinuclear Copper(II) Complexes: Synthesis, Structure, and Magnetic Properties of Complexes Derived from [1,3-propanediylbis(oxamato)]cuprate(II) ([Cu(pba)]²⁻). *Inorg. Chem.* **1993**, *32*, 3733–3742. [[CrossRef](#)]
37. Tercero, J.; Diaz, C.; el Fallah, M.S.; Ribas, J.; Solans, X.; Maestro, M.A.; Mahía, J. Synthesis, Characterization, and Magnetic Properties of Self-Assembled Compounds Based on Discrete Homotrimeric Complexes of Cu(II). *Inorg. Chem.* **2001**, *40*, 3077–3083. [[CrossRef](#)] [[PubMed](#)]
38. Gao, E.-Q.; Zhao, Q.-H.; Tang, J.-K.; Liao, D.-Z.; Jiang, Z.-H.; Yan, S.-P. A New One-Dimensional Coordination Polymer and a New Supramolecular Dimer Made of Trinuclear Copper(II) Complexes: Crystal Structure and Magnetic Properties. *J. Chem. Soc. Dalton Trans.* **2001**, *2001*, 1537–1540. [[CrossRef](#)]
39. Tercero, J.; Diaz, C.; Ribas, J.; Mahía, J.; Maestro, M.A. New Oxamato-Bridged Trinuclear Cu^{II}–Cu^{II}–Cu^{II} Complexes with Hydrogen-Bond Supramolecular Structures: Synthesis and Magneto–Structural Studies. *Inorg. Chem.* **2002**, *41*, 5373–5381. [[CrossRef](#)]
40. Pardo, E.; Bernot, K.; Julve, M.; Lloret, F.; Cano, J.; Ruiz-García, R.; Delgado, F.S.; Ruiz-Pérez, C.; Ottenwaelder, X.; Journaux, Y. Spin Control in Ladderlike Hexanuclear Copper(II) Complexes with Metallacyclophane Cores. *Inorg. Chem.* **2004**, *43*, 2768–2770. [[CrossRef](#)]
41. Pardo, E.; Ruiz-García, R.; Lloret, F.; Julve, M.; Cano, J.; Pasán, J.; Ruiz-Pérez, C.; Filali, Y.; Chamoreau, L.-M.; Journaux, Y. Molecular-Programmed Self-Assembly of Homo- and Heterometallic Penta- and Hexanuclear Coordination Compounds: Synthesis, Crystal Structures, and Magnetic Properties of Ladder-Type Cu^{II}₂M^{II}_x (M = Cu, Ni; x = 3, 4) Oxamato Complexes with Cu^{II}₂ Metallacyclophane Cores. *Inorg. Chem.* **2007**, *46*, 4504–4514. [[CrossRef](#)] [[PubMed](#)]
42. Rabelo, R.; Castellano, M.; Barros, W.P.; Carbonell-Vilar, J.M.; Viciano-Chumillas, M.; Lloret, F.; Julve, M.; Pasán, J.; Cañadillas-Delgado, L.; Ruiz-García, R.; et al. Molecular Engineering of an Inverse Hexacopper(II) Coordination Complex with a Photoactive Metallacyclophane Centroligand as Prototype of a Magnetic Photoswitch. *Polyhedron* **2022**, *217*, 115732. [[CrossRef](#)]
43. Pereira, C.L.M.; Pedroso, E.F.; Doriguetto, A.C.; Ellena, J.A.; Boubekour, K.; Filali, Y.; Journaux, Y.; Novak, M.A.; Stumpf, H.O. Design of 1D and 2D Molecule-Based Magnets with the Ligand 4,5-Dimethyl-1,2-Phenylenebis(Oxamato). *Dalton Trans.* **2011**, *40*, 746–754. [[CrossRef](#)] [[PubMed](#)]
44. Fettouhi, M.; Ouahab, L.; Boukhari, A.; Cador, O.; Mathonière, C.; Kahn, O. New Metal Oxamates as Precursors of Low-Dimensional Heterobimetallics. *Inorg. Chem.* **1996**, *35*, 4932–4937. [[CrossRef](#)] [[PubMed](#)]
45. Castro, I.; Faus, J.; Julve, M.; Amigó, J.M.; Sletten, J.; Debaerdemaeker, T. Copper(II)-Assisted Hydrolysis of 2,4,6-Tris(2-Pyridyl)-1,3,5-Triazine. Part 3. Crystal Structures of Diaqua[Bis(2-Pyridylcarbonyl)Amido]Copper(II) Nitrate Dihydrate and Aquabis(Pyridine-2-Carboxamide)Copper(II) Nitrate Monohydrate. *J. Chem. Soc. Dalton Trans.* **1990**, *1990*, 891–897. [[CrossRef](#)]
46. Macrae, C.F.; Sovago, I.; Cottrell, S.J.; Galek, P.T.A.; McCabe, P.; Pidcock, E.; Platings, M.; Shields, G.P.; Stevens, J.S.; Towler, M.; et al. Mercury 4.0: From visualization to analysis, design and prediction. *J. Appl. Crystallogr.* **2020**, *53*, 226–235. [[CrossRef](#)]
47. CrysAlis, P.R.O. *Xcalibur CCD System CrysAlis Software System*; Version 1.171.37.31; Rigaku Corporation: Tokyo, Japan, 2014.
48. Sheldrick, G.M. Crystal Structure Refinement with SHELXL. *Acta Crystallogr. C Struct. Chem.* **2015**, *71*, 3–8. [[CrossRef](#)]
49. Farrugia, L.J. WinGX and ORTEP for Windows: An Update. *J. Appl. Crystallogr.* **2012**, *45*, 849–854. [[CrossRef](#)]
50. Macrae, C.F.; Bruno, I.J.; Chisholm, J.A.; Edgington, P.R.; McCabe, P.; Pidcock, E.; Rodriguez-Monge, L.; Taylor, R.; van de Streek, J.; Wood, P.A. Mercury CSD 2.0—New Features for the Visualization and Investigation of Crystal Structures. *J. Appl. Crystallogr.* **2008**, *41*, 466–470. [[CrossRef](#)]
51. Bain, G.A.; Berry, J.F. Diamagnetic Corrections and Pascal’s Constants. *J. Chem. Educ.* **2008**, *85*, 532. [[CrossRef](#)]
52. Oliveira, W.X.C.; Pinheiro, C.B.; da Costa, M.M.; Fontes, A.P.S.; Nunes, W.C.; Lloret, F.; Julve, M.; Pereira, C.L.M. Crystal Engineering Applied to Modulate the Structure and Magnetic Properties of Oxamate Complexes Containing the [Cu(bpca)]⁺ Cation. *Cryst. Growth Des.* **2016**, *16*, 4094–4107. [[CrossRef](#)]
53. Simões, T.R.G.; Mambrini, R.V.; Reis, D.O.; Marinho, M.V.; Ribeiro, M.A.; Pinheiro, C.B.; Ferrando-Soria, J.; Déniz, M.; Ruiz-Pérez, C.; Cangussu, D.; et al. Copper(II) Assembling with Bis(2-Pyridylcarbonyl)Amidate and N,N′-2,2-Phenylenebis(Oxamate). *Dalton Trans.* **2013**, *42*, 5778–5795. [[CrossRef](#)]
54. Llunell, M.; Alemany, P.; Alvarez, S. *SHAPE*, Version 2.1; The Electronic Structure Groups: Barcelona, Spain, 2013.
55. Oliveira, W.X.C.; Ribeiro, M.A.; Pinheiro, C.B.; da Costa, M.M.; Fontes, A.P.S.; Nunes, W.C.; Cangussu, D.; Julve, M.; Stumpf, H.O.; Pereira, C.L.M. Palladium(II)–Copper(II) Assembling with Bis(2-Pyridylcarbonyl)Amidate and Bis(Oxamate) Type Ligands. *Cryst. Growth Des.* **2015**, *15*, 1325–1335. [[CrossRef](#)]
56. Castro, I.; Calatayud, M.L.; Orts-Arroyo, M.; Marino, N.; de Munno, G.; Lloret, F.; Ruiz-García, R.; Julve, M. Oxalato as Polyatomic Coordination Center and Magnetic Coupler in Copper(II)-Polypyrazole Inverse Polynuclear Complexes and Coordination Polymers. *Coord. Chem. Rev.* **2022**, *471*, 214730. [[CrossRef](#)]
57. Chilton, N.F.; Anderson, R.P.; Turner, L.D.; Soncini, A.; Murray, K.S. PHI: A Powerful New Program for the Analysis of Anisotropic Monomeric and Exchange-Coupled Polynuclear d- and f-Block Complexes. *J. Comput. Chem.* **2013**, *34*, 1164–1175. [[CrossRef](#)]

58. Kahn, O. *Molecular Magnetism*, 1st ed.; Wiley-VCH: New York, NY, USA, 1993; ISBN 978-0471188384.
59. Addison, A.W.; Rao, T.N.; Reedijk, J.; van Rijn, J.; Verschoor, G.C. Synthesis, Structure, and Spectroscopic Properties of Copper(II) Compounds Containing Nitrogen–Sulphur Donor Ligands; the Crystal and Molecular Structure of Aqua[1,7-Bis(N-Methylbenzimidazol-2'-yl)-2,6-Dithiaheptane]Copper(II) Perchlorate. *J. Chem. Soc. Dalton Trans.* **1984**, *1984*, 1349–1356. [[CrossRef](#)]
60. Baggio, R.; Garland, M.T.; Manzur, J.; Peña, O.; Perec, M.; Spodine, E.; Vega, A. A Dinuclear Copper(II) Complex Involving Monoatomic O-Carboxylate Bridging and Cu–S(Thioether) Bonds: [Cu(tda)(phen)]₂·H₂tda (tda = thiodiacetate, phen = phenanthroline). *Inorg. Chim. Acta* **1999**, *286*, 74–79. [[CrossRef](#)]
61. Greenaway, A.M.; O'Connor, C.J.; Overman, J.W.; Sinn, E. Magnetic Properties and Crystal Structure of an Acetate-Bridged Ferromagnetic Copper(II) Dimer. *Inorg. Chem.* **1981**, *20*, 1508–1513. [[CrossRef](#)]
62. Christou, G.; Perlepes, S.P.; Libby, E.; Folting, K.; Huffman, J.C.; Webb, R.J.; Hendrickson, D.N. Preparation and Properties of the Triply Bridged, Ferromagnetically Coupled Dinuclear Copper(II) Complexes [Cu₂(OAc)₃(bpy)₂](ClO₄) and [Cu₂(OH)(H₂O)(OAc)(bpy)₂](ClO₄)₂. *Inorg. Chem.* **1990**, *29*, 3657–3666. [[CrossRef](#)]
63. Baggio, R.; Calvo, R.; Garland, M.T.; Peña, O.; Perec, M.; Slep, L.D. A New Copper(II) Di-M2-Carboxylato Bridged Dinuclear Complex: [Cu(oda)phen]₂·6H₂O (oda = oxydiacetate, phen = phenanthroline). *Inorg. Chem. Commun.* **2007**, *10*, 1249–1252. [[CrossRef](#)]